Chapter 3
Electrostatics of Tubes, Wire Grids and Field Cages

The electric field in a drift chamber must provide two functions: drift and amplification. Whereas in the immediate vicinity of the thin proportional or 'sense' wire the cylindrical electric field provides directly the large field strengths required for charge amplification, the drift field must be created by a suitable arrangement of electrodes that are set at potentials supplied by external voltage sources. It is true that drift fields have also been created by depositing electric charges on insulators – such chambers are described in Sect. 11.4 – but we do not treat them here. Charge amplification is not necessarily confined to proportional wires. It has also been measured between parallel plates and between a wire mesh and a metal plate as well as in the tiny holes in a plate coated on both sides with the metal layers of a condenser. In fact these MICROMEGA and GEM counters seem to have a promising future [FAB 04].

There is a large variety of drift chambers, and they have all different electrode arrangements. An overview of existing chambers is given in Chap. 11, where we distinguish three basic types. In the volume-sensitive chambers (types 2 and 3) the functions of drift and amplification are often more or less well separated, either by special wire grids that separate the drift space from the sense wire or at least by the introduction of 'field' or 'potential' wires between the sense wires. The drift field, which fills a space large compared to the amplification space, then has to be defined at its boundaries; these make up the 'field cage'. For a uniform field, the electrodes at the boundaries are at graded potentials in the field direction and at constant potentials orthogonal to it.

Also the area-sensitive chambers (type 1) have often been built with 'potential' or 'field-shaping' wires to provide a better definition and a separate adjustment of the drift field. In this chapter we want to discuss some elements that are typical for the volume-sensitive chambers with separated drift and amplification spaces: one or several grids with regularly spaced wires in conjunction with a field cage. Although directly applicable to a time projection chamber (TPC), the following considerations will also apply to many type 2 chambers.

Electrostatic problems of the most general electrode configuration are usually solved by numerical methods, for example using relaxation techniques [WEN 58].

W. Blum et al., *Particle Detection with Drift Chambers*,

doi: 10.1007/978-3-540-76684-1_3,

Computer codes exist for wire chamber applications [VEN 08]. In this chapter we develop analytical methods taking advantage of simple geometry, in order to establish the main concepts. A classic treatment is found in Morse and Feshbach [MOR 53].

The simplest device for the measurement of drift time is the drift or proportional tube. This name refers to the original, proportional mode of amplification, but the device can also be used beyond the proportional mode, see Sect. 4.2. In its ideal form it is a circular cylindrical tube with a wire in the centre. As we have in mind to also describe deviations from the ideal form which arise in practice we will approach the electrostatics of a tube in a slightly generalized way.

3.1 Perfect and Imperfect Drift Tubes

Deviations from the ideal geometry of two concentric circular cylinders are caused by displaced wires or deformed walls. In this section we discuss the electric field arising in a circular right cylinder with the wire off-centre. Since we are dealing with relatively small deviations our method is a first-order perturbation calculation of the linear deviation.

The solution of Laplace's equation

$$\nabla^2 \Phi = 0 \tag{3.1}$$

for the potential Φ in the charge-free space between two conductors is found by separation of variables. In cylindrical coordinates we write

$$\begin{gathered} \Phi(r,\varphi,z) = R(r)\phi(\varphi)Z(z) \\ \frac{1}{rR}\frac{\partial}{\partial r}\left(r\frac{\partial R}{\partial r}\right) + \frac{1}{r^2\phi}\frac{\partial^2\phi}{\partial\varphi^2} + \frac{1}{Z}\frac{\partial^2 Z}{\partial z^2} = 0. \end{gathered} \tag{3.2}$$

Assuming $Z(z) = const = 1$, we equate the second term to the constant $-\nu^2$ so that

$$\frac{d^2\phi}{d\varphi^2} = -\nu^2\phi,$$

whose solutions are

$$\begin{aligned} \phi(\varphi) &= C'_\varphi \cos\nu\varphi + C''_\varphi \sin\nu\varphi \qquad && \text{if } \nu \neq 0 \\ \phi(\varphi) &= C'_\varphi\varphi + C''_\varphi && \text{if } \nu = 0. \end{aligned} \tag{3.3}$$

The C's are constants to be determined by the boundary conditions. The radial part becomes the Euler-Cauchy equation

$$r\frac{d}{dr}\left(r\frac{dR}{dr}\right) - \nu^2 R = 0. \tag{3.4}$$

If $\nu = 0$, the solution is given by

$$R(r) = C'_r \ln r + C''_r. \tag{3.5}$$

3.1.1 Perfect Drift Tube

The potential between two coaxial cylinders is a straight application of Eq. (3.5). When the outer cylinder (radius b) is on ground, and the wire (radius a) on positive potential U, one determines the coefficients to be given by $C'_\varphi = 0$, $C''_r = -C'_r \ln b$ and $C'_r C''_\varphi \ln(a/b) = U$, so that

$$\Phi = \frac{U}{\ln(a/b)} \ln(\frac{r}{b}). \tag{3.6}$$

The electric field is directed radially outwards, and

$$E_r = -\frac{\partial \Phi}{\partial r} = \frac{U}{\ln(b/a)} \frac{1}{r}. \tag{3.7}$$

Another way to calculate E_r is using Gauss' theorem according to which

$$E_r = \frac{\lambda}{2\pi\varepsilon_0} \frac{1}{r} \tag{3.8}$$

where λ is the linear charge density on the wire; the value of ε_0 is $8.854 \cdot 10^{-12}$ As/Vm. Therefore the capacitance per unit length of tube is given by

$$C = \frac{\lambda}{U} = \frac{2\pi\varepsilon_0}{\ln(b/a)}.$$

3.1.2 Displaced Wire

Solution of the Electrostatic Problem

Let the wire be displaced from the tube centre by the distance d in the negative y-direction (Fig. 3.1). The wire defines the centre of the coordinate system so that the first boundary condition is

$$\Phi(a) = U, \qquad \text{independent of } \varphi. \tag{3.9}$$

We must express the second boundary by the radius vector as a function of φ. The exact expression is

$$\rho = d \sin\varphi + b\sqrt{(1-(d^2/b^2)(1-\sin^2\varphi)},$$

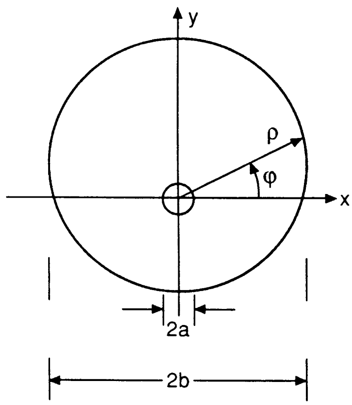

Fig. 3.1 Geometry of displaced wire

but we are only interested in small wire displacements. To first order in *d/b* we have the boundary at

$$\rho = b + d\sin\varphi, \tag{3.10}$$

and the second boundary condition is

$$\Phi(\rho) = 0. \tag{3.11}$$

Now we must determine the various coefficients using (3.9) and (3.11). To the first order in *d/b* we have solutions for $\nu = 0$ and $\nu = 1$, and the most general solution is

$$\Phi = (C_r^{0'} \ln r + C_r^{0''})C_\varphi^{0''} + (C_r^{1'} r + C_r^{1''}/r)(C_\varphi^{1'} \cos\varphi + C_\varphi^{1''} \sin\varphi). \tag{3.12}$$

Inserting (3.9), we have to require

$$C_r^{1'} a + C_r^{1''}/a = 0, \tag{3.13}$$

which implies that $C_r^{1''}$ can be neglected against $C_r^{1'}$ for the entire space except in the immediate vicinity of the wire surface.

When inserting (3.11) and (3.10) into (3.12) we make use of the relation

$$\ln(b + d\sin\varphi) = \ln b + (d/b)\sin\varphi,$$

which holds to first order in *d/b*. This determines the constants $C_r^{0'}$, $C_r^{0''}$ and $C_\varphi^{0''}$ as in the case (3.6) of the perfect tube. Comparing factors that multiply the $\sin\varphi$-terms, we find

$$C_\varphi^{0''} C_r^{0'} (d/b) + C_r^{1'} b C_\varphi^{1''} = 0$$

or

$$C_r^{1'} C_\varphi^{1''} = -\frac{d}{b^2} \frac{U}{\ln(a/b)} \tag{3.14}$$

whereas $C_\varphi^{1'} = 0$. This produces the solution, in first order of (*d/b*), equal to

$$\Phi(r,\varphi) = \frac{U}{\ln(a/b)} \ln\frac{r}{b} - \frac{U}{\ln(a/b)} \frac{d}{b} \frac{r}{b} \sin\varphi. \tag{3.15}$$

The perturbing potential Φ_1 caused by the wire displacement is given by the second term. Using $y = r\sin\varphi$, the field perturbation is calculated to be

$$(E_1)_y = -\frac{\partial \Phi_1}{\partial y} = -\frac{U}{\ln(b/a)}\frac{d}{b^2} \tag{3.16}$$

$$(E_1)_x = (E_1)_z = 0. \tag{3.17}$$

It describes a constant field directed towards negative y, whose magnitude is d/b times the value of the unperturbed field (3.7) at the wall.

For the purpose of calculating the electrostatic force on the wire (see further down) we also record the value of $(E_1)_y$ on the wire surface $(r = a)$. Starting from (3.13) without the previous simplification $C_r^{1''} = 0$, the correct perturbation potential is

$$\Phi_1(r,\varphi) = \frac{-U}{\ln(a/b)}\frac{d}{b^2}\left(r - \frac{a^2}{r}\right)\sin\varphi. \tag{3.18}$$

The field in y-direction equals

$$\begin{aligned} (E_1(a))_y &= -\frac{\partial \Phi_1}{\partial y} \qquad \text{evaluated at } r = a \\ &= -\frac{U}{\ln(b/a)}\frac{2d}{b^2}\sin^2\varphi \end{aligned}$$

Averaging over φ we have an extra field on the wire surface equal to

$$\overline{(E_1(a))_y} = -\frac{U}{\ln(b/a)}\frac{d}{b^2} \tag{3.19}$$

The average extra field on the wire surface is as large as the field perturbation (3.16), (3.17) throughout the volume.

Gravitational Sag

The main reason for wire displacement is the weight of the wire. Even when strung with a pulling force T close to the breaking limit, wires in several metre long tubes will experience a gravitational sag that is large in comparison with the achievable accuracy of drift tubes.

In order to derive a formula for the amount of bowing we introduce the coordinates y (downwards) and x (horizontal). We note that on every length element dx the weight of the wire is

$$\rho g \sigma \, dx \tag{3.20}$$

(ρ = density, σ = cross sectional area of the wire, $g = 981\,\mathrm{cm/s^2}$). It must be compensated by the vertical component of the tension at this point, which is equal to the difference of the slopes at the two ends of the interval dx, multiplied by the pulling force T:

$$-T[y'(x+dx) - y'(x)] \tag{3.21}$$

where the primes denote the first derivative. In this approximation we have assumed that the pulling force is the same for all x, the variation due to the weight of the wire being negligible for practical tubes.

Combining (3.20) and (3.21), one has the differential equation

$$-y'' = C = \rho g \sigma / T \tag{3.22}$$

with the solution

$$y = (C/2)x^2 + C_1 x + C_2. \tag{3.23}$$

Specifying that $y = 0$ at $x = \pm L/2$ determines the coefficients C_1, C_2, and the solution becomes

$$y = \frac{C}{2}\left(\frac{L^2}{4} - x^2\right). \tag{3.24}$$

The point of the maximum excursion is the sagitta, equal to

$$s = y(0) = \frac{CL^2}{8} = \frac{\rho g \sigma L^2}{8T}. \tag{3.25}$$

It is proportional to the inverse of the mechanical tension. If the tension is increased the sagitta is reduced, but the tension cannot be arbitrarily increased since non-elastic deformations take place. The maximum pulling force T_c that can be applied to a wire is proportional to its cross section, and the ratio T_c/σ is constant (except for very thin wires). The minimum achievable sagitta of a wire of given length is independent of the wire cross section. The values of the critical tension and typical sagittas for 100-cm-long wires of different materials are shown in Table 3.1. Usually the wires are strung to a tension close to the critical one in order to reduce the sagging. Inspecting Table 3.1 we notice that among the various materials, tungsten is the one that allows the smallest sagittas but at the expense of quite a large tension, for a given diameter of the wire. Since the tension of the wires is held by the endplates of the chamber, a large tension requires stiff endplates. In the design of a chamber one usually compromises between these two parameters.

If the sagitta of long wires cannot be constructed to be small one may be obliged to control its size within small tolerances. A practical way of doing this is by measuring the oscillation frequency of the wire. The frequency f_1 of the lowest mode of the elastic string is

Table 3.1 Maximum stresses before deformation of typical wire materials and corresponding sagittas for 1-m-long wires

Material	T_c/σ (kg/mm^2)	Sagitta (μm) of a 100 cm long wire strung at T_c
Al	4…16	21…84
Cu	21…37	30…53
Fe	18…25	39…54
W	180…410	6…13

$$f_1 = \frac{1}{2L}\sqrt{\frac{T}{\rho\sigma}}. \tag{3.26}$$

Inserting (3.25) into (3.26) produces the simple relation

$$f_1^2 = \frac{g}{32s}. \tag{3.27}$$

Electrostatic Force on the Sagged Wire

The displacement of the wire creates an average field (3.19) which acts on the electric charge of the wire and produces a force which tends to increase the displacement. The differential equation (3.22) needs to be complemented by a term which represents the electrostatic force per unit wire length. This is given by the product

$$\lambda \cdot \overline{(E_1(a))_y}$$

where λ is given by (3.8) in terms of the unperturbed field, and $\overline{(E_1(a))_y}$ is given by (3.19) and is proportional to the displacement y. The electrostatic force, like gravity, points downwards and leads to a positive term on the right-hand side of (3.22), whereas $y'' < 0$. Therefore, the differential equation is

$$y'' + k^2 y + C = 0 \tag{3.28}$$

with $C = \rho g \sigma / T$ and $k^2 = 2\pi\varepsilon_0 E_0^2(b)/T$. The value of k is plotted against $E_0(b)$ and T in Fig. 3.2.

The general solution of (3.28) is

$$y = C_1 \cos\, kx + C_2 \sin\, kx - C/k^2. \tag{3.29}$$

When specifying $y(\pm L/2) = 0$, the coefficients C_1, C_2 are determined, and the solution becomes

$$y = \frac{C}{k^2}\left(\frac{1}{\cos(kL/2)}\cos\, kx - 1\right). \tag{3.30}$$

The electrostatic force has changed the form of the wire from the parabola (3.24) to the cosine function (3.30).

The new sagitta is

$$s_k = y(0) = \frac{C}{k^2}\left(\frac{1}{\cos(kL/2)} - 1\right) \xrightarrow{kL \ll 1} \frac{CL^2}{8} \tag{3.31}$$

This means the electrostatic force has increased the sagitta (3.25) by the factor

$$\frac{s_k}{s} = \frac{8}{k^2L^2}\left(\frac{1}{\cos(kL/2)} - 1\right) = \frac{2}{q^2}\left(\frac{1}{\cos\, q} - 1\right). \tag{3.32}$$

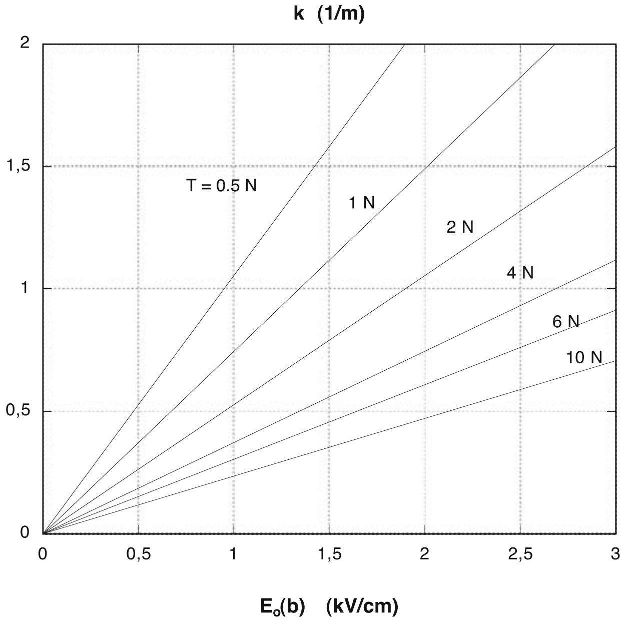

Fig. 3.2 Value of the constant k in (3.28) relevant for the electrostatic amplification of the gravitational sag, as a function of the electric field $E_0(b)$ at the tube wall, for various wire pulling forces T

As the product kL approaches the value π, the excursion tends to infinity, and the wire is no longer in a stable position. For example, the gravitational sag of a wire strung with one N inside a 5 m long tube will be amplified by a factor of s_k/s of 1.56 if the field at the wall is $E_0(b) = 500\text{V/cm}$. The point of instability is reached at $E_0(b) = 840\text{V/cm}$. In Fig. 3.3 we plot s_k/s as a function of q^2 or $k^2L^2/4$.

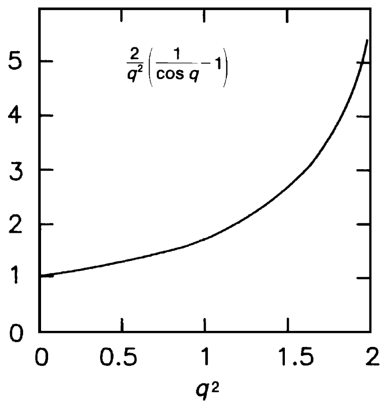

Fig. 3.3 Amplification factor of the gravitational sag owing to electrostatic forces, according to (3.32)

3.2 Wire Grids

3.2.1 The Electric Field of an Ideal Grid of Wires Parallel to a Conducting Plane

We assume a reference system with the $x-y$ plane coincident with the conducting plane (pad plane) and the y axis along the direction of the wires of the grid. The z axis is perpendicular to the plane (see Fig. 3.4).

The potential is a function of the coordinates x and z only, because the problem has a translational symmetry along the y direction. We assume the zero of the potential on the conducting plane $(z=0)$. The complex potential of a single line of charge λ per unit length placed at $U'=x'+\mathrm{i}z'$ is

$$\phi(U) = -\frac{\lambda}{2\pi\varepsilon_0}\ln\frac{(U-U')}{(U-\bar{U}')}, \tag{3.33}$$

where $U=x+\mathrm{i}z$ is the coordinate of a general point and $\bar{U}'=x'-\mathrm{i}z'$ is the complex conjugate of U'. MKS units are used throughout.

The potential of the whole grid is obtained by adding up the contributions of each wire:

$$\phi(U) = -\frac{\lambda}{2\pi\varepsilon_0}\sum_{k=-\infty}^{k=+\infty}\ln\frac{(U-U'_k)}{(U-\bar{U}'_k)},$$

where U'_k is the coordinate of the kth wire.

All the wires of the grid are equispaced with a pitch s: therefore

$$U'_k = x_0 + ks + \mathrm{i}z_0 (k=\ldots-2,-1,0,1,2,\ldots),$$

where x_0 and z_0 are the coordinates of the 0th wire of the grid. The potential of the grid can be written as

$$\phi(U) = -\frac{\lambda}{2\pi\varepsilon_0}\sum_{k=-\infty}^{k=+\infty}\ln\frac{(U-U'_0-ks)}{(U-\bar{U}'_0-ks)}.$$

This summation can be computed [ABR 65]:

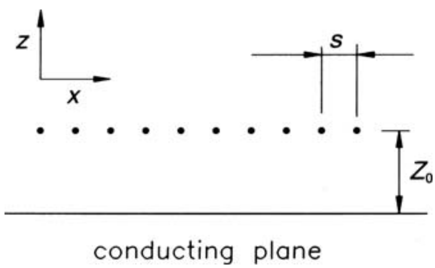

Fig. 3.4 An ideal grid of wires parallel to a conducting plane

$$\phi(U) = -\frac{\lambda}{2\pi\varepsilon_0} \ln \frac{\sin[(\pi/s)(U - U_0')]}{\sin[(\pi/s)(U - \bar{U}_0')]}$$

and the corresponding real potential is

$$\begin{aligned} V(x,z) &= \mathrm{Re}\ \phi(U) \\ &= -\frac{\lambda}{4\pi\varepsilon_0} \ln \frac{\sin^2[(\pi/s)(x - x_0)] + \sin\ \mathrm{h}^2[(\pi/s)(z - z_0)]}{\sin^2[(\pi/s)(x - x_0)] + \sin\ \mathrm{h}^2[(\pi/s)(z + z_0)]}. \end{aligned} \tag{3.34}$$

Figure 3.5a shows $V(x,\ z)$ as function of z at two different values of x. In the chosen example the grid was placed at $z_0 = s$. We notice that such a grid behaves almost everywhere like a simple layer of charge with surface density λ/s. Only in the immediate vicinity of the wires (distances much smaller than the pitch) can the structure of the grid be seen (compare with Fig. 3.5b, which shows the potential of a simple layer of charge). Therefore it is possible to superimpose different grids or plane electrodes at distances larger than the pitch without changing the boundary conditions of the electrostatic problem. We have an example of the general two-dimensional problem where a potential ϕ that varies periodically in one direction x has every Fourier component $\approx \cos(2\pi nx/s)$ damped along the transverse direction z according to the factor $\mathrm{e}^{-2\pi nz/s}$. This holds because every Fourier component must satisfy Laplace's equation

$$\frac{\partial^2\phi}{\partial x^2} + \frac{\partial^2\phi}{\partial z^2} = 0$$

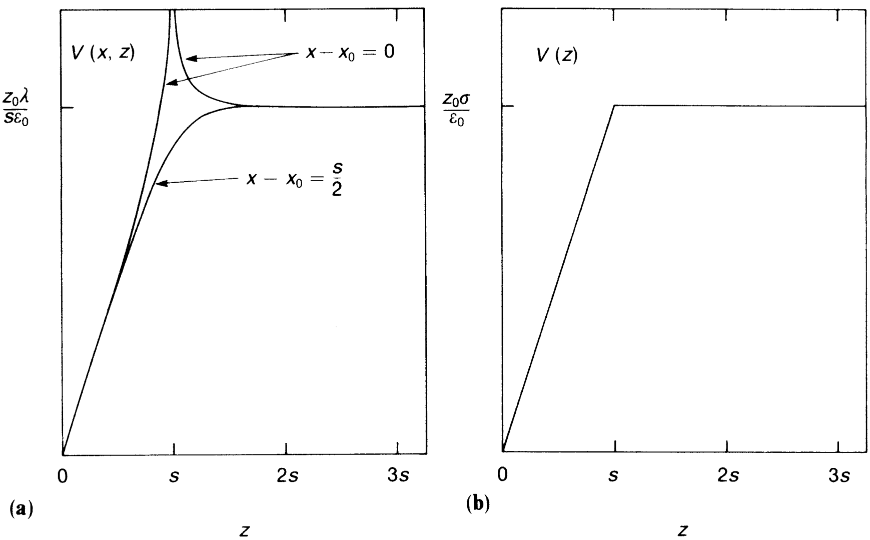

Fig. 3.5 (**a**) The potential $V(x,z)$ of a grid of wires situated a distance z_0 from a conducting plane at $x_0,\ x_0 + s, \ldots$ with pitch $s = z_0$ and a linear charge density λ per wire. (**b**) The potential $V(z)$ of a plane of charge situated a distance z_0 from a conducting plane, with a surface charge density σ

outside the wires. The solution is

$$\phi = \sum_n C_n \mathrm{e}^{-2\pi nz/s} \cos(2\pi nx/s),$$

the C_n being constants.

At a distance from the grid comparable or larger than the pitch the potential assumes the value

$$\begin{aligned} V(x,z) &= \frac{z\lambda}{\varepsilon_0 s} \quad \text{for } z < z_0, z_0 - z \gg \frac{s}{2\pi}, \\ V(x,z) &= \frac{z_0\lambda}{\varepsilon_0 s} \quad \text{for } z_0 < z, z - z_0 \gg \frac{s}{2\pi}. \end{aligned} \tag{3.35}$$

On the surface of the wires the potential assumes the value evaluated at $(x-x_0)^2 + (z-z_0)^2 = r^2$. We replace in first order of r/s the hyperbolic functions by their arguments and take for $\sinh(2\pi z_0/s)$ the positive exponential. The potential of the wire is then

$$V(\text{wire}) = \frac{\lambda z_0}{\varepsilon_0 s}\left(1 - \frac{s}{2\pi z_0} \ln \frac{2\pi r}{s}\right). \tag{3.36}$$

This means that the wire grid, although it behaves like a simple sheet with area charge density λ/s has some 'transparency'. We could have given the grid a zero potential and the conducting plane a potential V. Then, beyond the grid the potential would have been

$$\frac{\lambda}{2\pi\varepsilon_0} \ln \frac{2\pi r}{s}$$

and not zero as on the grid – some of the potential of the plane behind can be 'seen through the grid'. In other words, the potential beyond the grid is different from the potential on the grid by the difference between the electric field on the two sides of the grid, multiplied by the length $(s/2\pi)\ln(2\pi r/s)$.

The electric field that can be computed from (3.34) is given here for convenience:

$$E_x(x,z) = \frac{\lambda}{2s\varepsilon_0} \sin\left[\frac{2\pi}{s}(x-x_0)\right]\left[\frac{1}{A_1} - \frac{1}{A_2}\right],$$

$$E_z(x,z) = \frac{\lambda}{2s\varepsilon_0}\left\{\frac{\sinh[(2\pi/s)(z-z_0)]}{A_1} - \frac{\sinh[(2\pi/s)(z+z_0)]}{A_2}\right\},$$

where

$$A_1 = \cosh\left[\frac{2\pi}{s}(z-z_0)\right] - \cos\left[\frac{2\pi}{s}(x-x_0)\right],$$

$$A_2 = \cosh\left[\frac{2\pi}{s}(z+z_0)\right] - \cos\left[\frac{2\pi}{s}(x-x_0)\right].$$

3.2.2 Superposition of the Electric Fields of Several Grids and of a High-Voltage Plane

Knowing the potential created by one plane grid (3.34) and its very simple form (3.35) valid at a distance $d (d \gg s/2\pi)$ out of this plane, we want to be able to superimpose several such grids, in order to accommodate not only the sense wires but also all the other electrodes: the near-by field and shielding wires and the distant high-voltage electrode.

In order to be as explicit as possible we will present the specific case of a TPC. These chambers have more grids than most other volume-sensitive drift chambers, and the simpler cases may be derived by removing individual grids from the following computations.

We want to calculate the electric field in a TPC with the geometry sketched in Fig. 3.6. The pad plane is grounded, and we have four independent potentials: the high-voltage plane (V_p), the zero-grid wire (V_z), the field wires (V_f) and the sense wires (V_s). We have to find the relations between those potentials and the charge induced on the different electrodes.

Since the distance d between the grid planes satisfies the condition $d \gg s/2\pi$, the total electric field is generally obtained by superimposing the solution of each grid. This assumes that all the wires inside a single grid are at the same potential, but it is not the case for the sense-wire and field-wire grids where the sense wires and the field wires are at different potentials and the two grids are at the same z. In this case the superposition is still possible owing to the symmetry of the geometry: the potential induced by the sense-wire grid on the field wires is the same for all the field wires and vice-versa.

The potential induced by the sense-wire grid on the field wires can easily be computed because the field-wire grid and the sense-wire grid have the same pitch. Evaluating formula (3.34) at the position of any field wire we find that

$$V\left(x_0 + \frac{s_1}{2} + ks_1, z_1\right) = \frac{\lambda_\mathrm{s}}{2\pi\varepsilon_0} \ln\left[\cosh\frac{2\pi z_1}{s_1}\right] \approx \frac{\lambda_\mathrm{s} z_1}{\varepsilon_0 s_1} - \frac{\lambda_\mathrm{s}}{2\pi\varepsilon_0}\ln 2. \tag{3.37}$$

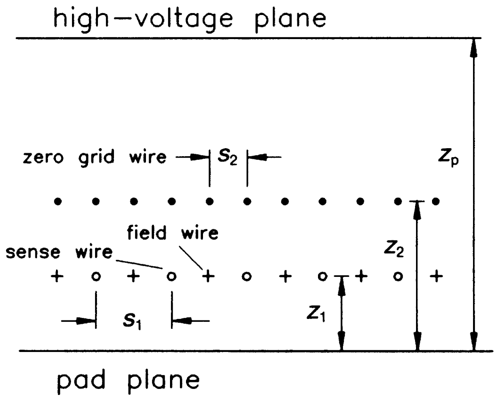

Fig. 3.6 Basic grid geometry of a TPC: The sense-wire/field-wire plane is sandwiched between two grounded planes – the zero-grid-wire plane and the pad plane. The high-voltage plane is a large distance away from them

We can now use (3.35), (3.36) and (3.37) to calculate the potential of each electrode as the sum of the contributions of the charges induced on each grid and on the high-voltage plane:

$$
\begin{aligned}
V_{\mathrm{s}} &= \frac{\lambda_{\mathrm{s}} z_1}{\varepsilon_0 s_1}\left(1-\frac{s_1}{2\pi z_1}\ln\frac{2\pi r_{\mathrm{s}}}{s_1}\right)+\frac{\lambda_{\mathrm{f}} z_1}{\varepsilon_0 s_1}\left(1-\frac{s_1}{2\pi z_1}\ln 2\right)+\frac{\lambda_{\mathrm{z}} z_1}{s_2\varepsilon_0}+\frac{\sigma_{\mathrm{p}} z_1}{\varepsilon_0}, \\
V_{\mathrm{f}} &= \frac{\lambda_{\mathrm{s}} z_1}{\varepsilon_0 s_1}\left(1-\frac{s_1}{2\pi z_1}\ln 2\right)+\frac{\lambda_{\mathrm{f}} z_1}{\varepsilon_0 s_1}\left(1-\frac{s_1}{2\pi z_1}\ln\frac{2\pi r_{\mathrm{f}}}{s_1}\right)+\frac{\lambda_{\mathrm{z}} z_1}{s_2\varepsilon_0}+\frac{\sigma_{\mathrm{p}} z_1}{\varepsilon_0}, \\
V_{\mathrm{z}} &= \frac{\lambda_{\mathrm{s}} z_1}{s_1\varepsilon_1}+\frac{\lambda_{\mathrm{f}} z_1}{s_1\varepsilon_0}+\frac{\lambda_{\mathrm{z}} z_2}{\varepsilon_0 s_2}\left(1-\frac{s_2}{2\pi z_2}\ln\frac{2\pi r_{\mathrm{z}}}{s_2}\right)+\frac{\sigma_{\mathrm{p}} z_2}{\varepsilon_0}, \\
V_{\mathrm{p}} &= \frac{\lambda_{\mathrm{s}} z_1}{s_1\varepsilon_0}+\frac{\lambda_{\mathrm{f}} z_1}{s_1\varepsilon_0}+\frac{\lambda_{\mathrm{z}} z_2}{s_2\varepsilon_0}+\frac{\sigma_{\mathrm{p}} z_{\mathrm{p}}}{\varepsilon_0},
\end{aligned}
\tag{3.38}
$$

where σ_{p} is the surface charge density on the high-voltage plane, $\lambda_{\mathrm{s}}, \lambda_{\mathrm{f}}, \lambda_{\mathrm{z}}$ are the charges per unit length on the wires, and $r_{\mathrm{s}}, r_{\mathrm{f}}, r_{\mathrm{z}}$ are the radii of the wires.

We can define a surface charge density σ, for each grid, as the charge per unit length, divided by the pitch (λ_i/s_i), and (3.38) can be written as

$$
\begin{pmatrix} V_{\mathrm{s}} \\ V_{\mathrm{f}} \\ V_{\mathrm{z}} \\ V_{\mathrm{p}} \end{pmatrix} = A \begin{pmatrix} \sigma_{\mathrm{s}} \\ \sigma_{\mathrm{f}} \\ \sigma_{\mathrm{z}} \\ \sigma_{\mathrm{p}} \end{pmatrix}, \tag{3.39}
$$

where A is the matrix of the potential coefficients. The matrix A can be inverted to give the capacitance matrix (this is the solution of the electrostatic problem):

$$
\begin{pmatrix} \sigma_{\mathrm{s}} \\ \sigma_{\mathrm{f}} \\ \sigma_{\mathrm{z}} \\ \sigma_{\mathrm{p}} \end{pmatrix} = A^{-1} \begin{pmatrix} V_{\mathrm{s}} \\ V_{\mathrm{f}} \\ V_{\mathrm{z}} \\ V_{\mathrm{p}} \end{pmatrix}. \tag{3.40}
$$

Once the capacitance matrix A^{-1} is known we can calculate the charges induced on each electrode for any configuration of the potentials. The electric field is given by the superposition of the drift field with the fields of all the grids, given by (3.38).

In normal operating conditions the electric field in the amplification region is much higher than the drift field. In this case $\lambda_{\mathrm{s}}/s_1 \gg |\sigma_{\mathrm{p}}|$ and the charge induced on the high-voltage plane can be approximated by

$$
\sigma_{\mathrm{p}} = \varepsilon_0 \frac{V_{\mathrm{p}} - V_{\mathrm{z}}}{z_{\mathrm{p}} - z_2}.
$$

Then the matrix A of (3.39) can be reduced to a 3×3 matrix, neglecting the last row and the last column,

Table 3.2 Matrix of the potential coefficients (m^2/farad) referring to the grids s, f and z in the standard case

$$A = 1.13 \times 10^8 \begin{pmatrix} 6.64 & 3.56 & 4.00 \\ 3.56 & 5.62 & 4.00 \\ 4.00 & 4.00 & 8.28 \end{pmatrix}$$

$$A = \frac{1}{\varepsilon_0} \begin{pmatrix} z_1 - \frac{s_1}{2\pi} \ln \frac{2\pi r_s}{s_1} & z_1 - \frac{s_1}{2\pi} \ln 2 & z_1 \\ z_1 - \frac{s_1}{2\pi} \ln 2 & z_1 - \frac{s_1}{2\pi} \ln \frac{2\pi r_f}{s_1} & z_1 \\ z_1 & z_1 & z_2 - \frac{s_2}{2\pi} \ln \frac{2\pi r_z}{s_2} \end{pmatrix}. \tag{3.41}$$

Tables 3.2 and 3.3 give the coefficients of the matrix A of (3.41) and of its inverse in a standard case:

$$z_1 = 4\,\text{mm},\ z_2 = 8\,\text{mm},\ s_1 = 4\,\text{mm},\ s_2 = 1\,\text{mm},$$
$$r_s = 0.01\,\text{mm},\ r_f = r_z = 0.05\,\text{mm}.$$

Using (3.38) we can now compute the potential of the high-voltage plane when it is uncharged ($\sigma_p = 0$):

$$V_p = V(\infty) = \sigma_s \frac{z_1}{\varepsilon_0} + \sigma_f \frac{z_1}{\varepsilon_0} + \sigma_z \frac{z_2}{\varepsilon_0}. \tag{3.42}$$

The electric field in the drift region is zero.

In order to produce a drift field E we have to set the high-voltage plane at a potential

$$V_p = -E(z_p - z_2) + V(\infty). \tag{3.43}$$

(E is defined positive and is the modulus of the drift field.)

3.2.3 *Matching the Potential of the Zero Grid and of the Electrodes of the Field Cage*

When we set the potential of the high-voltage plane V_p to the value defined by (3.43), the potential in the drift region ($z - z_2 \gg s_2/2\pi$) is given by

Table 3.3 Capacitance Matrix (farad/m^2) referring to the grids s, f and z in the standard case

$$A^{-1} = 8.85 \times 10^{-9} \begin{pmatrix} 0.25 & -0.11 & -0.07 \\ -0.11 & 0.32 & -0.10 \\ 0.07 & -0.10 & 0.21 \end{pmatrix}$$

$$V(z) = -E(z - z_2) + V(\infty). \tag{3.44}$$

Using equations (3.41) and (3.42) one can show that

$$V_z = V(\infty) - \frac{s_2}{2\pi\varepsilon_0}\sigma_z \ln\frac{\pi r_z}{s_2},$$

and (3.44) can be written as

$$V(z) = -E(z - z_2) + V_z + \frac{s_2}{2\pi\varepsilon_0}\sigma_z \ln\frac{2\pi r_z}{s_2}. \tag{3.45}$$

Figure 3.7 shows $V(z) - V_z$ as function of $z - z_2$ in the geometry discussed in the previous section with $V_s = 1300\,V, V_g = V_z = 0$ and with a superimposed drift field of 100 V/cm. We notice that in this configuration the equipotential surface of potential V_z is shifted into the drift region by about 2 mm. This effect has to be taken into account when the potential of the electrodes of the field cage has to be matched with the potential of the zero grid and when one has to set the potential of the gating grid (see Sect. 3.3.2).

After the adjustment of all the potentials on the grids and the high-voltage plane the field configuration is established. We show in Fig. 3.8 the field lines for the typical case of a TPC corresponding to Fig. 3.6 with $z_1 = 4\,\text{mm}$, $z_2 = 8\,\text{mm}$, $s_1 = 4\,\text{mm}$, $s_2 = 1\,\text{mm}$, $r_s = 0.01\,\text{mm}$, $r_f = r_z = 0.05\,\text{mm}$, $V_s = 1300\,\text{V}$, $V_f = V_z = 0$, $E_p = 100\,\text{V/cm}$. One observes that the drift region is filled with a very uniform

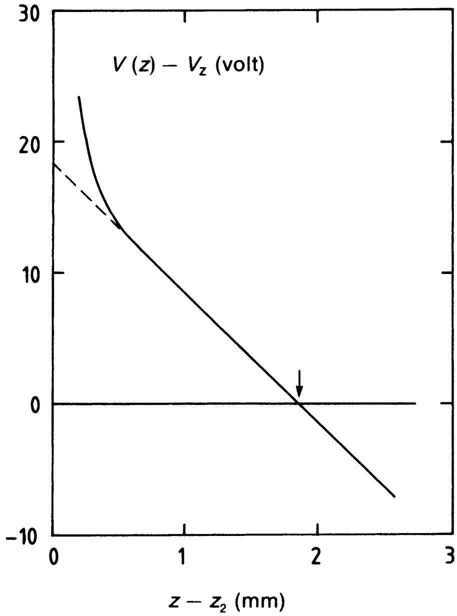

Fig. 3.7 Potential in the region of the zero grid as a function of z in presence of the drift field; example as discussed in the text

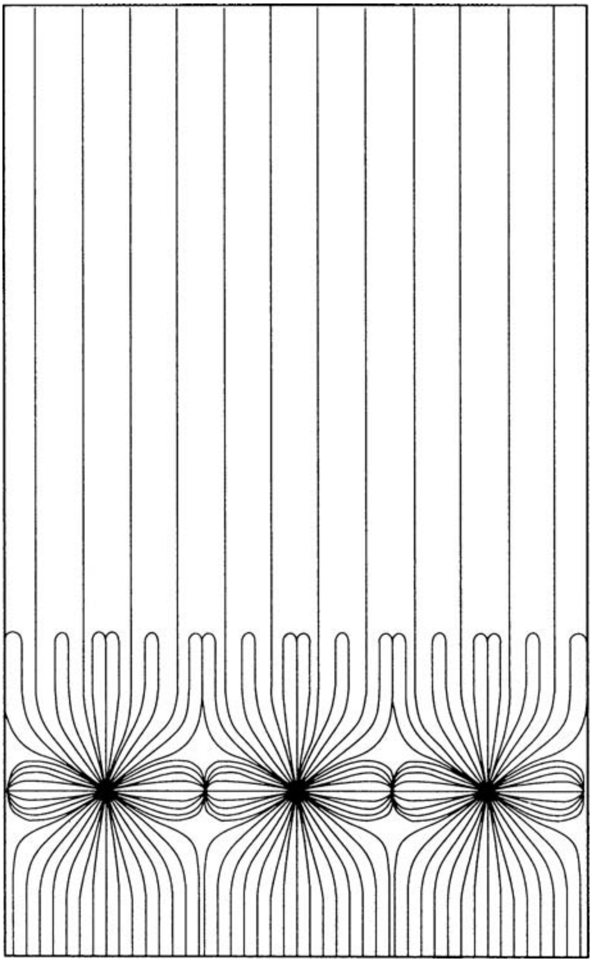

Fig. 3.8 Field lines for the typical case of a TPC with electrodes as in Fig. 3.6 $(z_1 = 4\,\text{mm},\ z_2 = 8\,\text{mm},\ s_1 = 4\,\text{mm},\ s_2 = 1\,\text{mm},\ r_\text{s} = 0.01\,\text{mm},\ r_\text{f} = r_\text{z} = 0.05\,\text{mm},\ V_\text{s} = 1300\,\text{V},\ V_\text{f} = V_\text{z} = 0,\ E_\text{p} = 100\,\text{V/cm})$

field, but also in the amplification region we find homogeneous domains as expected from (3.35). The electric field lines reach the sense wires from the drift region along narrow paths.

3.3 An Ion Gate in the Drift Space

It is possible to control the passage of the electrons from the drift region into the amplification region with a gate, which is an additional grid (‘gating grid’), located inside the drift volume in front of the zero grid and close to it. This is important when the drift chamber has to run under conditions of heavy background.

In this section we deal with the principal (electrostatic) function of the ion gate and how it is integrated into the system of all the other electrodes. Chapter 9 is devoted to a discussion of the behaviour of ion gates and their transparency under various operating conditions, including alternating wire potentials, and magnetic fields.

The potential of the wires of the gating grid can be regulated to make the grid opaque or transparent to the drifting electrons. In this section we neglect the effect of the magnetic field and assume that the electrons follow the electric field lines.

In the approximation that the electric field in the amplification region is much higher than the drift field, the variation of the potentials of the gating grid will not change appreciably the charge distribution on the electrodes in the amplification region, and we can schematize the gating grid as a grid of wires placed in between two infinite plane conductors: the high-voltage plane and the zero grid. The geometry is sketched in Fig. 3.9.

3.3.1 Calculation of Transparency

If the electrons follow the electric field lines we can compute the transparency T, i.e. the fraction of field lines that cross the gating grid, from the surface charge on the high-voltage plane and on the gating grid:

$$T = 1 - \frac{\sigma_g^+}{|\sigma_p|}, \tag{3.46}$$

where σ_p is the surface charge density on the high-voltage plane (negative) and σ_g^+ is the surface charge density of positive charges on the gating grid.

If we approximate the wires of the grid by lines of charge λ per unit length, the surface charge density on the grid is simply λ/s, and the condition of full transparency is

$$\lambda \leq 0.$$

This approximation is no longer correct when the absolute value of λ is so small that we have to consider the variation of charge density over the surface of the wire. A wire 'floating' in an external electric field E is polarized by the field, which

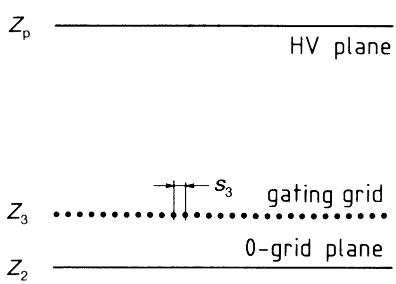

Fig. 3.9 Scheme for the inclusion of the gating grid

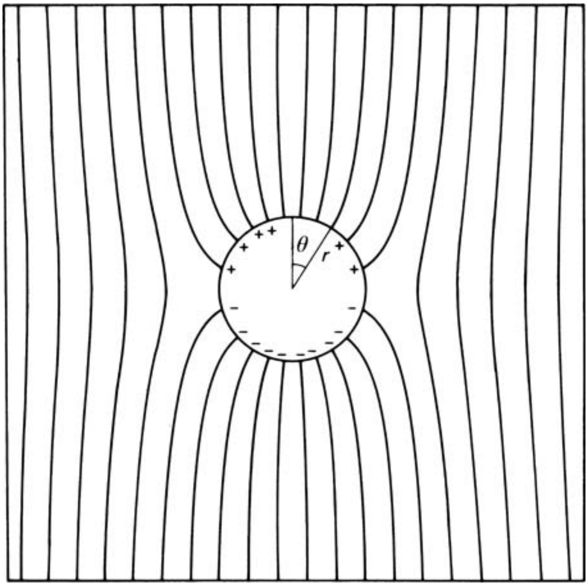

Fig. 3.10 Electric field lines near an uncharged wire floating in a homogenous field

produces a surface charge density σ_D on the wire. It depends on the azimuth (see Fig. 3.10):

$$\sigma_D = 2E\varepsilon_0 \cos\theta, \tag{3.47}$$

where θ is the angle between E and the radius vector from the centre to the surface of the wire [PUR 63].

In the general case the wire has, in addition to this polarization charge, a linear charge λ. The total surface charge density on the wire is

$$\sigma_w = \frac{\lambda}{2\pi r} + 2E\varepsilon_0 \cos\theta, \tag{3.48}$$

r being the radius of the wire. An illustration is Fig. 3.11. When

$$\frac{|\lambda|}{4\pi\varepsilon_0} \gg Er$$

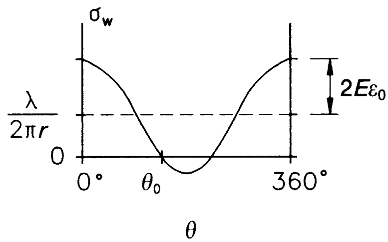

Fig. 3.11 Dependence on azimuth of the surface charge density σ_w located on the gating grid wire

the polarization effect can be neglected. This is the case of the zero-grid, sense and field wires, as discussed in the previous section.

There may be both positive and negative charges on the wires of the gating grid. In order to calculate T we must now count the positive charges only. This can be done using (3.48):

$$\begin{aligned}
\lambda^+ &= 0 && \text{when} \quad \frac{\lambda}{2\pi r} < -2E\varepsilon_0, \\
\lambda^+ &= \lambda && \text{when} \quad \frac{\lambda}{2\pi r} > 2E\varepsilon_0, \\
\lambda^+ &= \frac{\lambda\theta_0}{\pi} + 4E\varepsilon_0 r \sin\theta_0 && \\
& && \text{when} \; -2E\varepsilon_0 < \frac{\lambda}{2\pi r} < 2E\varepsilon_0, \\
\theta_0 &= \arccos\frac{-\lambda}{4\pi\varepsilon_0 E r}
\end{aligned} \tag{3.49}$$

and the surface charge density of positive charge on the gating grid is

$$\sigma_g^+ = \frac{\lambda^+}{s_3}. \tag{3.50}$$

Using (3.46) and (3.50) we obtain the condition for full transparency in the general case:

$$\frac{\lambda_g}{2\pi r_g} \leq -2E\varepsilon_0 \quad \text{or} \quad \frac{\sigma_g}{2\pi r_g} s_3 \leq -2E\varepsilon_0. \tag{3.51}$$

In the limiting condition of full transparency, the electric field between the gating grid and the zero-grid increases by a factor

$$1 + 4\pi\frac{r_g}{s_3}$$

with respect to the drift field.

Using (3.50) and (3.50) we can calculate the transparency in the special case of $\sigma_g = 0$:

$$T = 1 - \frac{4r_g}{s_3}.$$

The opacity of the gating grid in this configuration is twice the geometrical opacity. To illustrate the situation of limiting transparency the field lines above and below the fully open gate are displayed in Fig. 3.12a,b.

The drift field lines for our standard case are shown in Fig. 3.13a,b. We observe that the drifting electrons arrive on a sense wire on one of four roads through the zero grid – a consequence of the ratio of $s_1/s_3 = 4$.

In order to compute the transparency as a function of the gating-grid potential we have to calculate the capacity matrix. Following the scheme of Sect. 3.2 we obtain

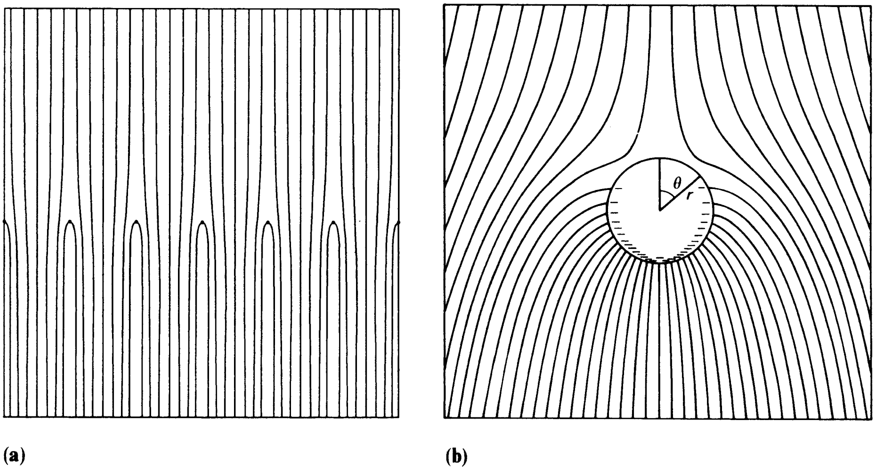

Fig. 3.12a,b Field lines in the limiting case of full transparency. **(a)** Neighbourhood above and below the gate (the electrons drift from above), **(b)** Enlargement around the region around one wire

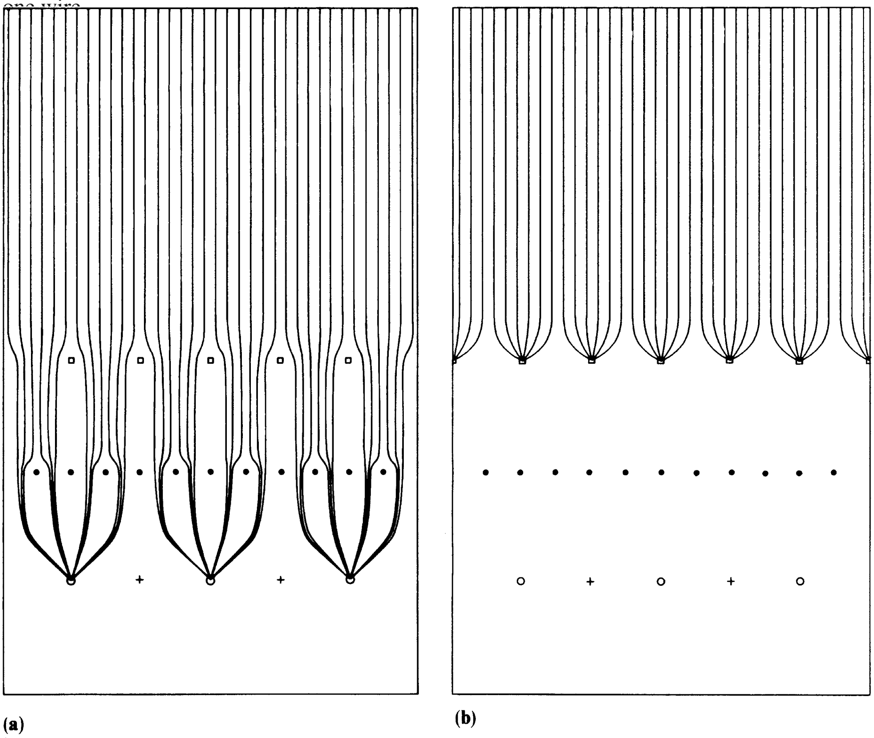

Fig. 3.13a,b Drift field lines in a standard case ($z_1 = 4\,\mathrm{mm}$, $z_2 = 8\,\mathrm{mm}$, $z_3 = 12\,\mathrm{mm}$, $s_1 = 4\,\mathrm{mm}$, $s_2 = 1\,\mathrm{mm}$, $s_3 = 2\,\mathrm{mm}$). The field lines between the sense wires and the other electrodes have been omitted for clariy. *Squares*: gating grid; *black circles*: zero-grid; *open circles*: sense wires; *crosses*: field wires, **(a)** gating grid open (maximal transparency), **(b)** gating grid closed

$$\begin{pmatrix} V_p - V_z \\ V_g - V_z \end{pmatrix} = \frac{1}{\varepsilon_0} \begin{pmatrix} z_p - z_2 & z_3 - z_2 \\ z_3 - z_2 & (z_3 - z_2) - \dfrac{s_3}{2\pi} \ln \dfrac{2\pi r_g}{s_3} \end{pmatrix} \begin{pmatrix} \sigma_p \\ \sigma_g \end{pmatrix} \tag{3.52}$$

and

$$\begin{pmatrix} \sigma_p \\ \sigma_g \end{pmatrix} = K \begin{pmatrix} z_3 - z_2 - \dfrac{s_3}{2\pi} \ln \dfrac{2\pi r_g}{s_3} & -(z_3 - z_2) \\ -(z_3 - z_2) & z_p - z_2 \end{pmatrix} \begin{pmatrix} V_p - V_z \\ V_g - V_z \end{pmatrix}, \tag{3.53}$$

where

$$K = \frac{\varepsilon_0}{(z_p - z_2)\left(z_3 - z_2 - \dfrac{s_3}{2\pi} \ln \dfrac{2\pi r_g}{s_3}\right) - (z_3 - z_2)^2}$$

and V_g is the potential of the gating grid. In the following we neglect the second term in the denominator of the factor K, since $z_p - z_2 \gg z_3 - z_2$ in the standard case.

Using (3.51) and (3.53) we can calculate the minimum value of V_g needed for the full transparency of the gating grid:

$$V_g - V_z \leq \frac{4\pi r_g}{s_3} \frac{V_p - V_z}{z_p - z_2} \left(z_3 - z_2 - \frac{s_3}{2\pi} \ln \frac{2\pi r_g}{s_3}\right) + \frac{z_3 - z_2}{z_p - z_2}(V_p - V_z). \tag{3.54}$$

The second term of (3.54) is the potential difference that makes $\sigma_g = 0$. The first term is the additional difference needed to eliminate the positive charges from the gating grid. In a standard configuration the two terms are comparable.

In Fig. 3.14 we compare the transparency calculated according to (3.46–3.53) for our standard case with measurements performed on a model of the ALEPH TPC [AME 85-1]. There is good agreement between theory and experiment.

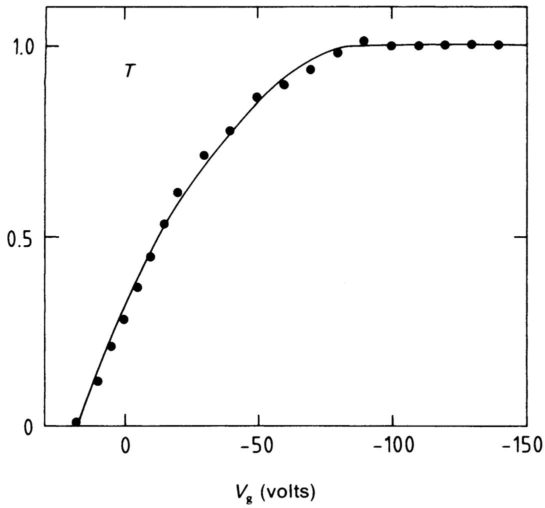

Fig. 3.14 Electron transparency of a grid with pitch 2 mm, as a function of the common potential V_g applied to the wires. The electrode configuration corresponds to Fig. 3.6. The points represent measurements by [AME 85-1]. The line is a function calculated using (3.46–3.54)

3.3.2 Setting of the Gating Grid Potential with Respect to the Zero-Grid Potential

In Sect. 3.4 it was shown that because of the high field in the amplification region the average potential at the position of the zero-grid does not coincide with V_z. The potential in the drift region, where the gating grid has to be placed, is given by (3.45).

This formula can be extrapolated at $z = z_2$:

$$V(z_2) = V_\mathrm{z} + \frac{s_2}{2\pi\varepsilon_0}\sigma_\mathrm{z} \ln \frac{2\pi r_\mathrm{z}}{s_2}, \tag{3.55}$$

giving the effective potential of the zero-grid seen from the region where the gating grid has to be placed.

In Sect. 3.3.1 we calculated the condition of full transparency, approximating the zero-grid as a solid plane at a potential V_z and referring to it the potential of the gating grid. In the real case V_g has to be referred to the effective potential $V(z_2)$ given by (3.55).

From what has been shown so far one can deduce that by making V_g sufficiently positive all drift field lines terminate on the gating grid and the transparency T is 0. Figure 3.13a,bb shows how the drift field lines terminate on the gating grid.

3.4 Field Cages

The electric field in the drift region has to be as uniform as possible and ideally similar to that of an infinitely large parallel-plate capacitor. The ideal boundary condition on the field cage is then a linear potential varying from the potential of the high-voltage membrane to the effective potential of the zero-grid.

This boundary condition can be constructed, in principle, by covering the field cage with a high-resistivity uniform material. A very good approximation can be obtained covering the inner surface of the field cage with a regular set of conducting strips perpendicular to the electric field, with a constant potential difference ΔV between two adjacent strips:

$$\Delta V = E\Delta,$$

where Δ is the pitch of the electrode system.

The exact form of the electric field produced by this system of electrodes can be calculated with conformal mapping taking advantage of the symmetry of the boundary conditions [DUR 64]. Figure 3.15 shows the electric field lines and the equipotentials near the strips in a particular case when the distance between two strips is 1/10 of the strip width. The electric field very near to the strips is not uniform and there are also field lines that go from one strip to the adjacent one. The transverse component essentially decays as $\exp(-2\pi t/\Delta)$ where t is the distance from the field cage (see Sect. 3.2), and when $t = \Delta$ the ratio between the transverse and the main component of the electric field is about 10^{-3}. At larger distances it

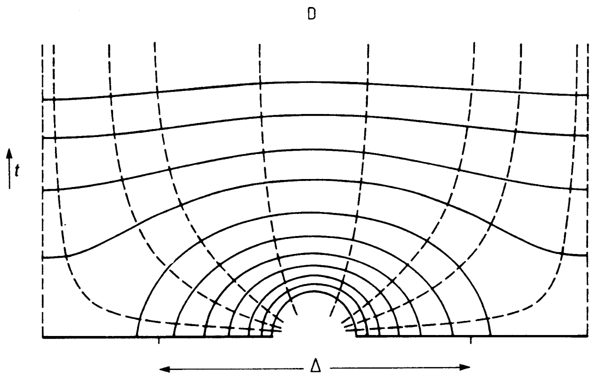

Fig. 3.15 Electric field configuration near the strips of a field cage. Equipotential lines (*broken*) and electric field lines (*full*) are shown. D: drift space; Δ: electrode pitch; t: coordinate in the drift space

becomes completely negligible, showing that this geometry of the electrodes is indeed a good approximation of the ideal case. However, the insulators present some problems.

3.4.1 The Difficulty of Free Dielectric Surfaces

The Dirichlet boundary conditions of the electrostatic problem to be solved in some volume require the specification of a potential at every point of a closed boundary surface. When conducting strips are involved that are at increasing potentials, insulators between them are unavoidable, and the potential on these cannot be specified. If the amount of free charge deposited on these surfaces were known everywhere, one would have mixed boundary conditions, partly Dirichlet, partly Neumann, and a solution could be found. In high-voltage field cages there is always some gas ionization, and the amount of free charges ready to deposit on some insulator is infinitely large. How can this uncertainty in the definition of the drift field be limited? There are several solutions to this difficulty:

Controlled (*small, surface or volume*) *conductivity of the insulator*: For every rate of deposit of ions there is some value of conductivity allowing the transport of these ions sufficiently fast to the next electrode, so that their disturbing effect is limited.

Retracted insulator surfaces: If the electrodes have the form indicated in Fig. 3.16a,ba or b, any field E that may develop at the bottom of the ditch between conductors owing to charge deposit will be damped by a factor of the order of $\exp(-\pi d/s)$ at the edge of the drift space. (For details of this electrostatic problem, see e.g. [JAC 75, p. 72.]) A maximum field E is given by the breakdown strength of the particular gas.

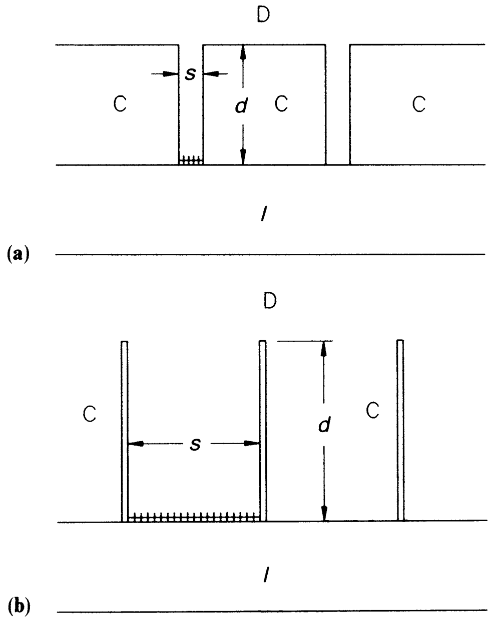

Fig. 3.16a,b Field-cage electrode configuration with retracted insulator surfaces. I: insulator, C: conductor, D: drift space, **(a)** small gap, **(b)** large gap

Thin insulator with shielding electrodes covering the gap from behind: Apart from the system of main electrodes, there is another set separated by a thin layer of insulator, and staggered by a half-step according to Fig. 3.17. The purpose of these shielding electrodes at intermediate potentials is to regularize the field in the drift region, but also to produce virtual mirror charges of any free charges that may have deposited in the gap, thus reducing their effect in the drift space.

If we assume that by one of the measures described above the adverse effects of any charge deposit are sufficiently reduced, we may imagine a smooth (linear) transition of potential between neighbouring electrodes, and the exact form of the electric field produced by the system of electrodes at increasing potentials can be calculated as discussed at the beginning of this section.

Electrostatic distortions were studied by Iwasaki et al. [IWA 83].

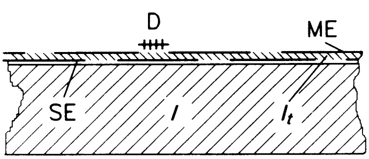

Fig. 3.17 Field-cage electrode configuration with secondary electrode strips (SE) covering the gaps between the main electrode strips (ME) behind a thin insulator foil (It). D: drift space; I: insulator

3.4.2 Irregularities in the Field Cage

In this subsection we present some studies that have arisen in practice when estimating the tolerances that had to be respected in the ALEPH TPC for the conductivity of the insulator, for the match of the gating grid and for the resistors in the potential divider. We quote the three relevant electrostatic solutions as examples of similar problems in chambers with different geometry.

If all the electrodes of the field cage are set at the correct potential, the drift field is uniform and parallel to the axis of the TPC in the whole drift volume. A wrong setting of the potentials produces a transverse component of the electric field and causes a distortion of the trajectories of the drifting electrons. In order to study this effect in detail the drift volume of the TPC is schematized as a cylinder of length L and radius A (see Fig. 3.18). The potentials defined on the surface of the cylinder define the boundary conditions of the electrostatic problem and the drift field inside the volume. If the potentials on the boundary do not vary with ϕ, the electric field can only have a transverse component in the radial direction.

In the absence of magnetic field the electrons drift along the electric field line; an electron placed at the position $(r_0,\ z_0)$ reaches the end of the drift volume at a radial position

$$r = r_0 + \int_{z_0}^{0} \frac{E_{\mathrm{r}}(r,z)}{E_z}\mathrm{d}z.$$

The radial component of the field can be calculated solving the Poisson equation in cylindrical coordinates [JAC 75, p. 108]. Since the ideal setting of the potential does not produce radial electric field components it is convenient to use as a boundary condition the difference between the actual and the ideal potentials. This is possible because the Poisson equation is linear in the potential. Although we discuss the examples in a cylindrical geometry, they apply to other geometries in a similar way.

Non-Linearity in the Resistor Chain. The potential of the strips of the field cage are defined connecting them to a linear resistor chain. The strips are insulated from the external ground by an insulator that has a finite resistivity and that is in parallel with the resistors of the chain. It can be shown that the resistance to ground of a strip placed at a position z is

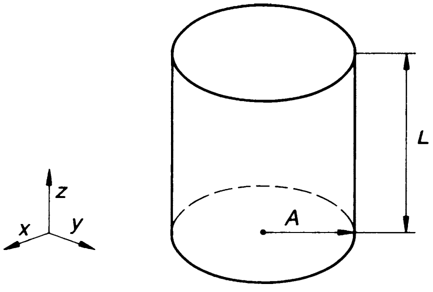

Fig. 3.18 Scheme of a cylindrical TPC drift region

$$R(z) = R_{\text{tot}} \left[\frac{z}{L} - \frac{1}{6} \left(\frac{z}{L} \right)^3 \frac{R_{\text{tot}}}{R_{\text{man}}} \right],$$

where R_{tot} is the resistance of the whole resistor chain and R_{man} is the resistance of the insulator mantel across the wall of the insulator. This non-linear resistance produces a potential distribution that differs from the linear one by

$$\Delta V(z) = \left[\frac{Z}{L} - \left(\frac{Z}{L} \right)^3 \right] V_{\text{p}} \frac{R_{\text{tot}}}{R_{\text{man}}} \frac{R_{\text{tot}}}{R_{\text{man}}} \ll 1,$$

where V_{p} is the potential of the central electrode. This error potential can be approximated by

$$\Delta V(z) \approx \frac{0.38}{6} V_{\text{p}} \frac{R_{\text{tot}}}{R_{\text{man}}} \sin\left(\pi \frac{z}{L} \right).$$

Following Jackson's formalism [JAC 75] it can be shown that the radial displacement of an electron drifting from the point $(r,\ z)$ is

$$\Delta r \approx \frac{0.38}{6} \frac{R_{\text{tot}}}{R_{\text{man}}} L \frac{\mathrm{i} J_1 \left(\frac{\mathrm{i}\pi r}{L} \right)}{J_0 \left(\frac{\mathrm{i}\pi A}{L} \right)} \cos\left(\frac{\pi z}{L} - 1 \right),$$

where J_0 are the Bessel functions of order 0 and 1. Figure 3.19 shows a plot of Δr as function of z for different values of r assuming $L = A = 2\,\text{m}$ and $R_{\text{tot}}/R_{\text{man}} = 10^{-3}$.

Mismatch of the Gating Grid. The potentials of the field cage have to match that of the last wire plane as discussed in Sect. 3.2. An error ΔV in the potential of the last electrode of the field cage produces a radial displacement

$$\Delta r = 2L \frac{\Delta V}{V_{\text{p}}} \sum_n \frac{J_1(x_n r/A)}{J_1(x_n) x_n} \left(\frac{\cosh[\pi(L-z)(x_n/A) - \cosh(L x_n/A)}{\sinh(L x_{n/A})} \right),$$

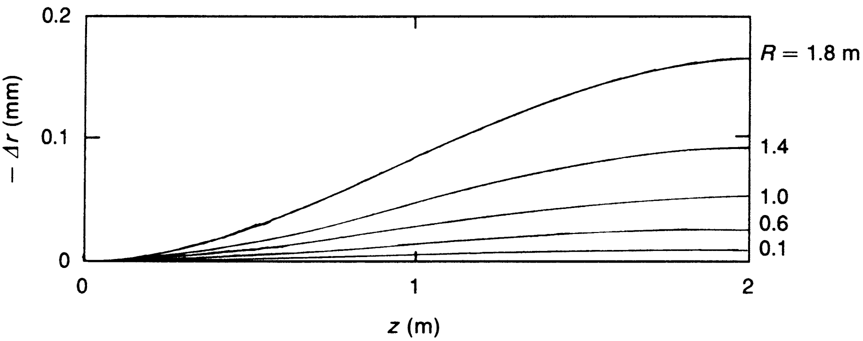

Fig. 3.19 Radial displacement r of the arrival point of an electron, caused by a resistance R_{man} of the insulator mantle a thousand times the value of the resistor chain, Δr is shown as a function of the starting point z, R in the example $A = L = 2\,\text{m}$

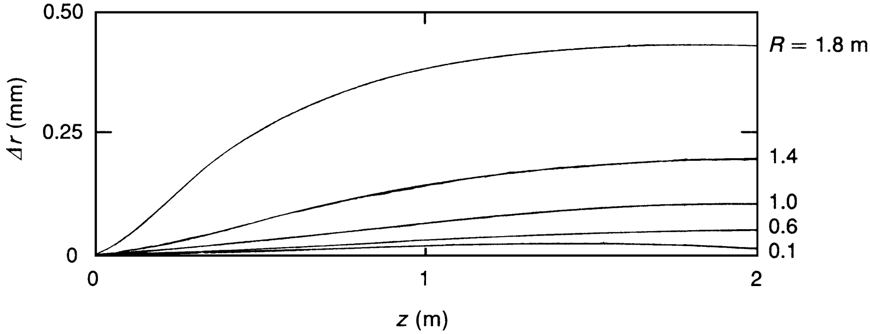

Fig. 3.20 Radial displacement Δr of the arrival point of an electron, caused by a voltage mismatch ΔV between the last electrode of the field cage and the last wire plane, amounting to $\Delta V/V_{\mathrm{p}} = 10^{-4}$ of the drift voltage. Δr is shown as a function of the starting point (z, R) in the example $A = L = 2\,\mathrm{m}$

where $x_n = k_n A$ and $J_0(k_n) = 0$.

Figure 3.20 shows a plot of Δr as a function of z for different values of r assuming $L = A = 2\,\mathrm{m}$ and $\Delta V/V_{\mathrm{p}} = 10^{-4}$.

Resistor Chain Containing One Wrong Resistor. If in the voltage-divider chain one of the resistors (placed at $z = \bar{z}$) has a wrong value, it induces an error in the potential of the field cage:

$$\begin{aligned} \Delta V(z) &= \frac{-\Delta V}{L} z, \quad z < \bar{z}, \\ \Delta V \left(1 - \frac{z}{L}\right), & \qquad z > \bar{z}, \\ \Delta V &= V_{\mathrm{p}} \frac{\Delta R}{R_{\mathrm{tot}}}, \end{aligned}$$

where ΔR is the error in the resistance of that particular resistor and R_{tot} is the total resistance of the chain. The induced radial displacement is

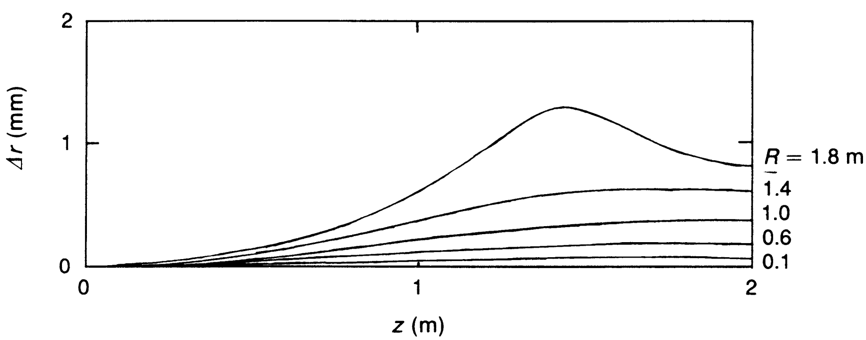

Fig. 3.21 Radial displacement Δr of the arrival point of an electron, caused by one wrong resistor value $R^* = R + \Delta R$, where $\Delta R/R_{\mathrm{tot}} = 1/400$ of the value of the total resistor chain. Δr is shown as a function of the starting point (z, R) in the example $A = L = 2\,\mathrm{m}$

$$\Delta r = L\frac{\Delta R}{r_{\text{tot}}}\left[\frac{1}{\pi}\sum\frac{\mathrm{i}J_1(\mathrm{i}n\pi r)/L}{J_0(\mathrm{i}n\pi A)/L}\frac{1}{n}\cos\left(\frac{n\pi\bar{z}}{L}\right)\left(\cos\frac{n\pi z}{L}-1\right)\right].$$

Figure 3.21 shows a plot of Δr as a function of z for different values of r for a particular case $L = A = 2\,\mathrm{m}$, $z = 1.4\,\mathrm{m}$, $\Delta R/R_{\text{tot}} = 1/400$.

We have computed in this subsection three specific cases of field-cage problems in the spirit of showing the order of magnitude of the relevant electron displacements. The design of the drift chamber must be such that the displacement Δr induced by such irregularities remains small in comparison to the required accuracy.

References

[ABR 65] M. Abramowitz and I.A. Stegun, *Handbook of Mathematical Functions*, (Dover, New York 1965) p. 75

[AME 85-1] S.R. Amendolia et al., Influence of the magnet field on the gating of a time projection chamber, *Nucl. Instrum. Methods A* **234**, 47 (1985)

[DUR 64] Durand, *Electrostatique* vol. II (Masson et C. edts., Paris 1964)

[FAB 04] C.W. Fabjan and W. Riegler, Trends and Highlights of VCI 2004, *Nucl. Instr. Meth. Phys. Res. A* **535**, p. 79-87 (2004)

[IWA 83] H. Iwasaki, R.J. Maderas, D.R. Nygren, G.T. Przybylski, and R.R. Sauerwein, Studies of electrostatic distortions with a small time projection chamber, in *The Time Projection Chamber* (A.I.P. Conference Proceedings No. 10 TRIUMF, Vancouver, Canada, 1983)

[JAC 75] J.D. Jackson, *Classical Electrodynamics* (Wiley, New York 1975)

[MOR 53] P.M. Morse and H. Feshbach, *Methods of Theoretical Physics* (McGraw Hill, New York 1953).

[PUR 63] E.M. Purcell, *Electricity and Magnetism* (Berkeley Physics Course Vol. II, McGraw Hill, New York 1963) Problem 9.11

[VEN 08] R. Veenhof, *Drift Chamber Simulation Program Garfield*, (1984–2008)

[WEN 58] G. Wendt, Statische Felder und stationäre Ströme in *Handbuch der Physik*, Vol. XVI (Springer, Berlin Heidelberg 1958) p. 148